Soft Matter

Cite this: *Soft Matter*, 2012, **8**, 9676

www.rsc.org/softmatter

PAPER

Water-soluble, stable helical polypeptide-grafted cyclodextrin bioconjugates: synthesis, secondary and self-assembly structures, and inclusion complex with guest compounds†

Yung-Chih Lin, Po-I Wang and Shiao-Wei Kuo*

Received 5th April 2012, Accepted 19th July 2012
DOI: 10.1039/c2sm25804h

In this study, we synthesized a linear copolymer, poly(γ-propargyl-L-glutamate-*graft*-cyclodextrin) (PPLG-*g*-CD), through Huisgen [2 + 3] cycloadditions (click reactions) of monoazido-functionalized β-cyclodextrin (N_3-CD) with the propargyl side chains, obtaining a self-assembling structure with a highly stable α-helical conformation and water-solubility. We used Fourier transform infrared spectroscopy, solid state nuclear magnetic resonance spectroscopy, wide-angle X-ray diffraction, and circular dichroism analyses in the solid state and in solution to characterize the transformations of the secondary structures between α-helix and β-sheet conformations. Temperature-dependent FTIR spectroscopic analyses revealed that the presence of the CD units on the PPLG side chain increased the stability of the α-helix conformation toward elevated temperatures, relative to that of pure PPLG. In addition, the presence of the CD cavities allowed the grafted polymers to form inclusion complexes with low-molecular-weight compounds, providing macromolecules with potential biomedical applications.

Introduction

Polypeptides are interesting materials because of their close relationship to proteins, flexible range of functionality, molecular recognition properties, and drug delivery applications.[1,2] The latter typically require water-soluble components to enhance circulation *in vivo*.[3] Polypeptides form hierarchically ordered structures containing α-helices and β-sheets, two secondary structures that are both stabilized through intra- and intermolecular hydrogen bonding, respectively.[4] Conformational studies of model polypeptides provide us with a means of mimicking the biological activities of more-complex proteins, because the secondary structures of peptide chains influence the well-defined tertiary structures of proteins.[1]

The α-helical structures of some polypeptides [*e.g.*, poly(γ-benzyl L-glutamate) (PBLG)] result in the formation of rigid rods that can exhibit liquid crystalline ordering in concentrated solutions and cast films;[5–7] they are often employed as model rigid rod systems in solution and in the solid state,[6–8] providing unique bulk[9,10] and solution[9–12] behavior. The design of water-soluble α-helical polypeptides, mimicking biologically active peptides, is often problematic; a high proportion of hydrophobic side chains (*e.g.*, benzene rings in PBLG) is necessary to enhance hydrogen bonding between the C=O groups and the amide linkages of the α-helical conformation, but it might result in a structure exhibiting low water-solubility.[13,14] Cheng *et al.* prepared polypeptides with long side chains bearing charged groups through thiol–ene click reactions of a γ-(4-allyloxybenzyl)-L-glutamate *N*-carboxyanhydride monomer; these systems were highly water-soluble and highly helical, even when the degree of polymerization (DP) was as low as 10.[15] Nevertheless, polyelectrolytes featuring charged peptide residues will display pH-dependent solubility and limited circulation lifetime, due to aggregation with oppositely charged biopolymers.[16] Nonionic yet water-soluble polypeptides featuring stable α-helical conformations are, therefore, attractive materials for biomedical applications. The grafting of poly(ethylene glycol) (PEG) onto a polypeptide through direct modification of a peptide *N*-carboxyanhydride monomer is typically the method used to improve the behavior of the polypeptide *in vivo*.[17] Deming *et al.* prepared the first examples of nonionic, water-soluble PEG-functionalized polylysines.[16] In addition, the attachment of azide-terminated PEG to poly(γ-propargyl-L-glutamate) (PPLG) through click reactions is also a highly efficient means of grafting onto a polypeptide side chain and maintaining its α-helical conformation.[18,19] High-molecular-weight polypeptides are necessary to ensure completely α-helical conformations in solution; at low DPs (*e.g.*, <18), PBLG exhibits three secondary structures (α-helix, β-sheet, random coil), with the rigid α-helical secondary structure favored when the DP increases.[4,20] In addition, the ether functionalities of the PEG moieties make these systems quite impractical for interaction, through noncovalent bonding, with guest compounds (*e.g.*, drugs).

Department of Materials and Optoelectronic Science, Center for Nanoscience and Nanotechnology, National Sun Yat-Sen University, Kaohsiung, 804, Taiwan. E-mail: kuosw@faculty.nsysu.edu.tw

† Electronic supplementary information (ESI) available. See DOI: 10.1039/c2sm25804h

Stronger noncovalent bonds, including electrostatic, hydrogen bonding, and host–guest interactions, have been utilized for the biological delivery of many compounds, including drugs, genes, proteins, and imaging agents.[21,22]

In this paper, we report new nonionic, water-soluble, highly functionalized (for host–guest interactions) polypeptides, exhibiting stable α-helical conformations, prepared through click reactions of an azide-functionalized β-cyclodextrin (β-CD) with several PPLG oligomers (Scheme 1). These new PPLG-*g*-CD systems were highly water-soluble and displayed high helicity even when the DP was as low as 5. CDs are among the most popular host molecules employed in molecular assemblies. They are cyclic oligosaccharides consisting of six (α), seven (β), or eight (γ) glucose units linked through 1,4-α-glucosidic bonds.[23] With their rigid, well-defined ring structures and cone-shaped cavities, CDs have the ability to act as hosts for a wide variety of molecular guests,[24] which can vary from lipophilic small molecules [*e.g.*, adamantane, pyrene (Py)][25–27] to macromolecules [*e.g.*, PEG, polycaprolactone].[28–31] In this study, we characterized the secondary structures and self-assembled inclusion complexes (ICs) of PPLG and PPLG-*g*-CD using Fourier transform infrared (FTIR) spectroscopy, solid state nuclear magnetic resonance (NMR) spectroscopy, wide-angle X-ray diffraction (WAXD), circular dichroism, and photoluminescence (PL) emission spectroscopy.

Experimental

Materials

Propargyl alcohol and L-glutamic acid were purchased from Tokyo Kasei Kogyo. Copper(I) bromide (CuBr) was purified by washing with glacial AcOH overnight, washing with absolute EtOH and ethyl ether, and then drying under vacuum. Sodium azide (NaN_3), triethylamine (TEA), *N*,*N*-dimethylformamide (DMF), *N*,*N*,*N*′,*N*″,*N*″-pentamethyldiethylenetriamine (PMDETA, 99%), Py, β-CD, and toluenesulfonyl chloride (TsCl, 98%) were purchased from Aldrich. All solvents were distilled prior to use. γ-Propargyl-L-glutamate[32,33] and mono-[6-*O*-(*p*-tolylsulfonyl)]-β-cyclodextrin (β-CD-OTs)[34] were prepared according to previously reported procedures.

Mono-(6-azido-6-desoxy)-β-cyclodextrin (β-CD-N_3)[34]

β-CD-OTs (1.10 g, 0.864 mmol) was added to a solution of NaN_3 (1.62 g, 24.9 mmol) in water (40 mL) and then the mixture was heated at 90 °C overnight. After cooling to room temperature, the clear solution was poured into acetone (400 mL); the precipitate was filtered off and dried under high vacuum to yield a white solid (0.802 g, 80%). ^{1}H NMR (DMSO-d_6): δ 3.24–3.44 (br overlapped, 14H, H-b,d), 3.50–3.72 (br overlapped, 28H, H-c,e,f), 3.75 (s, 2H, H-g), 4.42–4.57 (m, 6H, OH-f), 4.77–4.89 (d, 7H, H-a), 5.59–5.81 (br overlapped, 14H, OH-b,c). FTIR: 3386s (OH), 2926m (CH), 2106m (azide), 1647m, 1419m, 1153s, 1080s (OH), 1029vs (CH), 945w (Fig. S1 and S2†).

Ring-opening polymerization of *N*-carboxyanhydride (PPLG)[32,33]

γ-Propargyl-L-glutamate *N*-carboxyanhydride (PLG-NCA) was frozen in liquid N_2 under vacuum. DMF was added as a solvent *via* syringe and then the solution was warmed to 0 °C. N_2 gas was introduced into the reactor. The initiator compound containing amino groups was added and stirred for 48 h at a lower temperature. The residual polypeptide was collected by removing the solvent under vacuum. The solid residue was dissolved in DMF and precipitated with cold diethyl ether or MeOH. The pure polymer products were filtered off and the solid was dried under vacuum at room temperature (Table 1, Fig. S3 and S4†).

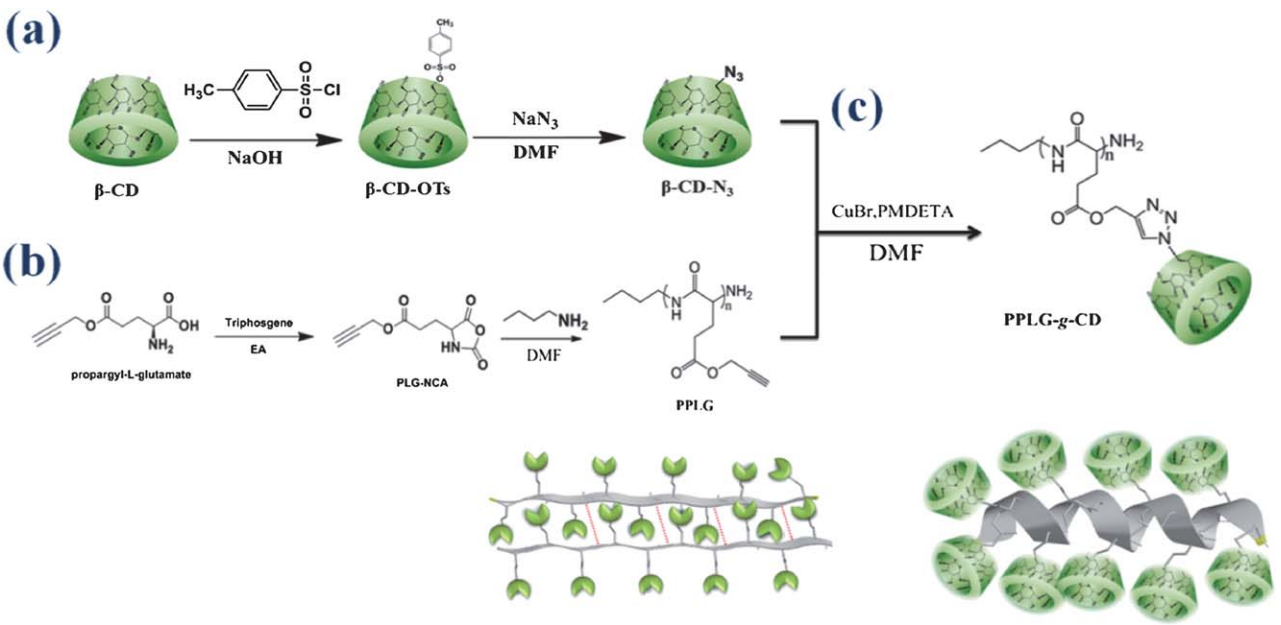

Scheme 1 Synthesis of PPLG-*g*-CD copolymers.

Table 1 PPLG-*g*-CD species prepared in this study

Polymer	M_n[a]	M_n[b]	PDI[b]
$PPLG_5$	910	3090	1.07
$PPLG_{10}$	1740	5750	1.16
$PPLG_{30}$	5080	6890	1.13
$PPLG_5$-CD	6580	3150	1.06
$PPLG_{10}$-CD	13 100	13 770	1.06
$PPLG_{30}$-CD	39 100	31 200	1.08

[a] Determined from ^{1}H NMR spectra. [b] Determined from GPC analysis.

Water-soluble PPLG-*g*-CD copolymers

β-CD-N_3 (2.27 g, 2 mmol), PPLG (0.200 g, 1.20 mmol), and CuBr (0.17 g, 1.18 mmol) were dissolved in DMF (40 mL) in a flask equipped with a magnetic stirrer bar. After one brief freeze–thaw–pump cycle, PMDETA (24.64 μL, 1.180 mmol) was added. The reaction mixture was then carefully degassed through three freeze–thaw–pump cycles, placed in an oil bath thermostated at 60 °C, and stirred for 24 h. After evaporating all of the solvent under reduced pressure, the residue was dissolved in THF and passed through a neutral alumina column to remove the copper catalysts. The concentrated THF solvent was evaporated and then the product was precipitated in MeOH. The precipitate was filtered off and dried under vacuum at room temperature, yielding the linear PPLG-*g*-CD as a white powder. ^{1}H NMR (TFA-*d*): δ 2.24–2.66 (d, 2H, H-d), 2.94 (s, 2H, H-c), 4.23–4.57 (d, 1H, H-e), 5.24–5.50 (t, 2H, H-g), 5.50–5.83 (m, 2H, H-b), 8.7 (s, 1H, H-a). FTIR: 3367s (OH), 2927m (CH), 1734m (free C═O), 1664s (C═O), 1541m (C═O), 1388m, 1260m, 1157s, 1080s (OH), 1030vs (CH), 945w. The chemical reaction and the results are summarized in Scheme 1 and Table 1.

Characterization

^{1}H NMR spectra were recorded at room temperature using a Bruker AM 500 (500 MHz) spectrometer, with the residual proton resonance of the deuterated solvent acting as the internal standard. High-resolution solid state NMR spectra were recorded at room temperature using a Bruker DSX-400 spectrometer operated at resonance frequencies of 399.53 and 100.47 MHz for ^{1}H and ^{13}C nuclei, respectively. ^{13}C cross-polarization (CP)/magic angle sample spinning (MAS) spectra were measured using a 3.9 μs 90° pulse, a 3 s pulse delay time, a 30 ms acquisition time, and 2048 scans. All NMR spectra were recorded at 300 K using broad band proton decoupling and a normal CP pulse sequence. Molecular weights and molecular weight distributions were determined through gel permeation chromatography (GPC) using a Waters 510 high-performance liquid chromatograph (HPLC) equipped with a 410 differential refractometer and three Ultrastyragel columns (100, 500, and 10^3 Å) connected in series, with DMF as the eluent (flow rate: 0.4 mL min^{-1}). Thermal analysis through differential scanning calorimetry (DSC) was performed using a TA-Q20 instrument operated at a scan rate of 10 °C min^{-1} over a temperature range from −90 to +200 °C under a N_2 atmosphere. FTIR spectra of the polymer films were recorded using the conventional KBr disk method. The films used in this study were sufficiently thin to obey the Beer–Lambert law. FTIR spectra were recorded using a Bruker Tensor 27 FTIR spectrophotometer; 32 scans were collected at a spectral resolution of 1 cm^{-1}. Circular dichroism spectra were recorded using a JASCO J-810 spectrometer, with sample in deionized water or MeOH at a concentration of 1 mg mL^{-1}. Mass spectra were obtained using a Bruker Daltonics Autoflex III MALDI-TOF mass spectrometer. The following voltage parameters were employed: ion source 1, 19.06 kV; ion source 2, 16.61 kV; lens, 8.78 kV; reflector 1, 21.08 kV; and reflector 2, 9.73 kV. X-ray diffraction (XRD) data were collected on the wiggler beamline BL17A1 of the National Synchrotron Radiation Research Center (NSRRC), Taiwan. A triangular bent Si (111) single crystal was employed to obtain a monochromated beam with a wavelength (λ) of 1.33001 Å. The XRD patterns were collected using an imaging plate (IP; Fuji BAS III; area = 20 × 40 cm^2) curved with a radius equivalent to the sample-to-detector distance (280 mm). The two-dimensional (2D) XRD patterns observed for the sample (typical diameter: 10 mm; thickness: 1 mm) were circularly averaged to obtain a one-dimensional (1D) diffraction profile $I(Q)$. The value of Q was calibrated using standard samples of silver behenate and Si powder (NBS 640b). Photoluminescence (PL) excitation and emission spectra were collected at room temperature using a monochromatized Xe light source.

Results and discussion

Synthesis of water-soluble PPLG-*g*-CD copolymers

Fig. 1 presents the ^{1}H NMR spectra of PPLG, N_3-CD, and PPLG-*g*-CD. The signal for the proton on the nitrogen atom of PPLG appeared as a singlet at 8.41 ppm [Fig. 1(a)]; the singlets at 2.50 and 4.78 ppm correspond to the *H*C≡C–C and C≡ C–C*H*$_2$ protons, respectively. The other alkyl CH_2 protons appeared upfield as multiplets between 2.0 and 2.6 ppm. The signals of the butyl group of the butylamine initiator were located at 0.95, 1.40, 1.60, and 3.38 ppm.[35,36] The signal of the CH_2 group connected to the azide unit of N_3-CD appeared at 3.88 ppm; it shifted downfield significantly to 3.95 ppm for PPLG-*g*-CD. In addition, signals for the CD moiety also appeared in the spectrum of PPLG-*g*-CD. The resonance at 8.5 ppm was due to the protons of the triazole structures resulting from the click reaction, confirming the successful synthesis of PPLG-*g*-CD. Fig. 2 presents the ^{13}C NMR spectra of PPLG, N_3-CD, and PPLG-*g*-CD. The ^{13}C NMR spectrum of $PPLG_{10}$ in *d*-TFA reveals signals for the C═O and amide carbon atoms at 177 and 175 ppm, respectively, while those of the alkyne carbon atoms remain at 77 ppm. The signals for the amino acid α-carbon atoms (NHCO*C*) appear at 55.7 ppm; Fig. 2(c) provides assignments of the remaining signals for the carbon atoms of PPLG. The signals of the C═O and amide carbon atoms appear in the ^{13}C NMR spectrum of PPLG-*g*-CD at 172.0 and 175.0 ppm, respectively; those of the N_3-CD unit appear at 104.6, 83.7, 76.3, 72.5, and 68.6 ppm. The signals for the carbon atom *C*-j and α-carbon atom *C*-n of PPLG-*g*-CD appear at 68.0 and 56.1 (α-helical conformation), respectively; signals for the alkane carbon atoms from butylamine are also evident. The signals of the alkyne carbon atoms of PPLG, which appeared at 77.0 ppm, were absent in the spectrum of PPLG-*g*-CD, but two new peaks appeared at 132.9 and 141.0 ppm, representing the carbon atoms of the triazole structures formed through the click reactions, confirming the successful synthesis of PPLG-*g*-CD. FTIR spectroscopic analysis revealed the complete

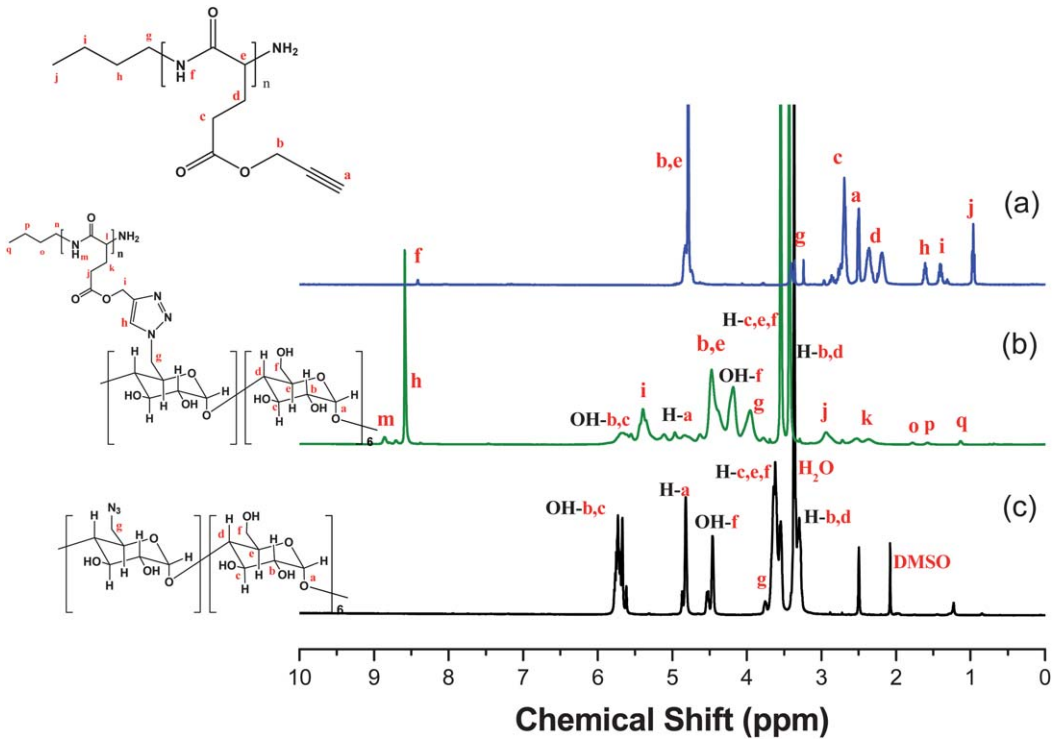

Fig. 1 ^{1}H NMR spectra of (a) $PPLG_{10}$, (b) $PPLG_{10}$-CD (in *d*-TFA), and (c) β-CD-N_3 (in *d*-DMSO).

disappearance of the characteristic signals for the azido and acetylene groups (Fig. 3). The signals at 2130 cm^{-1}, representing the acetylene group of PPLG, and 2105 cm^{-1}, representing the azide group of N_3-CD, were absent in the spectrum of PPLG-*g*-CD. A broad signal for the OH groups of the CD moiety at 3370 cm^{-1} and a signal for the amide I groups of the PPLG at 1660 cm^{-1} appeared in the spectrum of PPLG-*g*-CD, confirming that the azido and acetylene functionalities had participated in click reactions. The well-defined structure was confirmed in the corresponding MALDI-TOF MS spectra (Fig. 4), which revealed only one apparent distribution for both PPLG and PPLG-*g*-CD. The mass differences between all adjacent pairs of

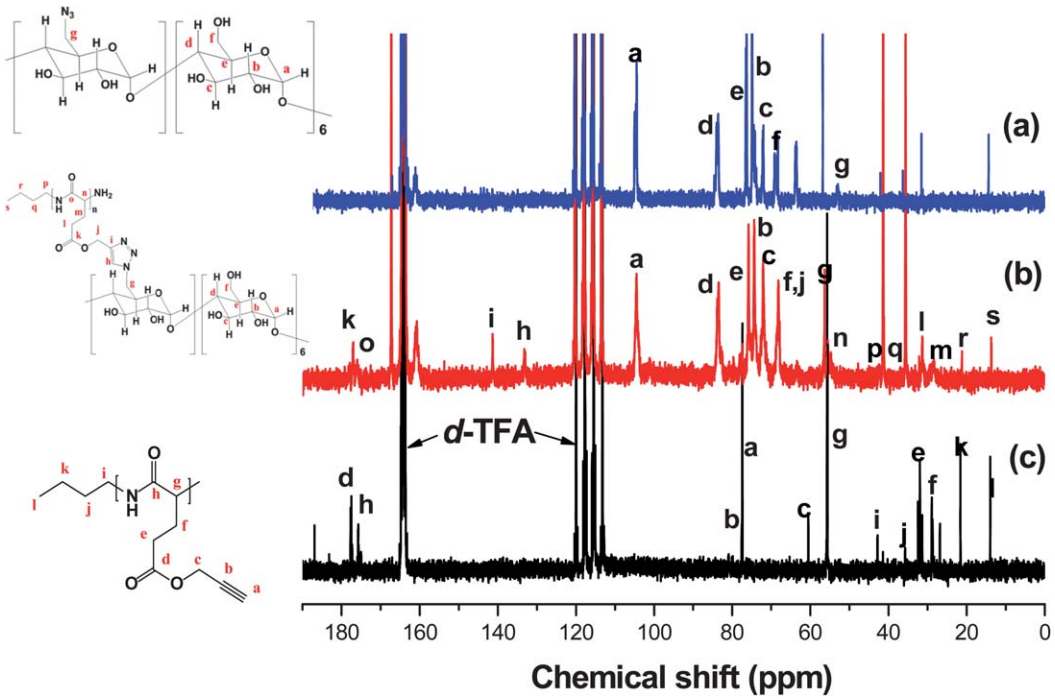

Fig. 2 ^{13}C NMR spectra of (a) β-CD-N_3, (b) $PPLG_{10}$-*g*-CD, and (c) $PPLG_{10}$ (in *d*-TFA).

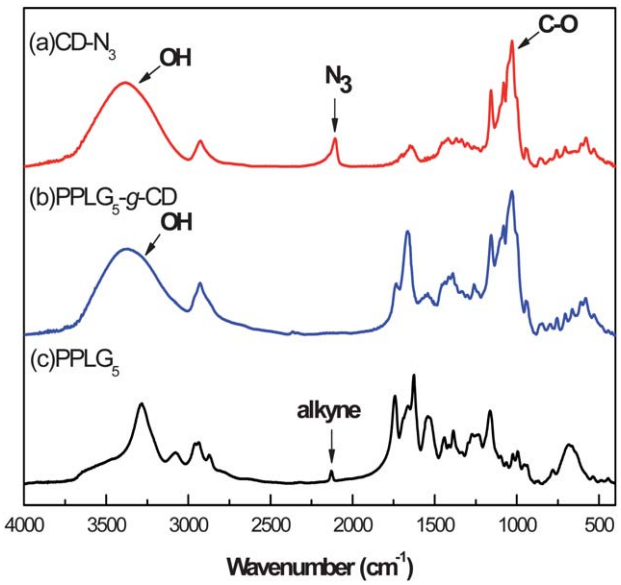

Fig. 3 FTIR spectra of (a) CD-N_3, (b) $PPLG_5$-*g*-CD, and (c) $PPLG_5$.

peaks were *m*/*z* 167 for PPLG and *m*/*z* 1327 for PPLG-*g*-CD, as expected for the repeating units of PPLG and PPLG-*g*-CD, respectively. Taken together, the data from the ^{1}H NMR, ^{13}C NMR, and FTIR spectra and the MALDI-TOF mass spectra confirmed the successful synthesis of PPLG-*g*-CD.

Conformation of the peptide segment

We recorded FTIR spectra at room temperature to obtain information regarding the conformations of the peptide segments of PPLG and PPLG-*g*-CD (Fig. 5). Analysis of these spectra using the second-derivative technique revealed (Fig. 6) that the amide I band at 1655 cm^{-1} was characteristic of an α-helical secondary structure. For polypeptides possessing a β-sheet conformation, the amide I band was located at 1627 cm^{-1}; random coil or turn populations were characterized by a signal at 1693 cm^{-1}. The free C═O unit of the side chain group of PPLG provided a signal at 1740 cm^{-1} (Fig. 6). Next, we used the deconvolution technique in a series of Gaussian distributions to quantify the fraction of each of the peaks (inset to Fig. 6). Fig. 7 summarizes our results obtained from curve fitting of the amide I group for the β-sheet, α-helical, and random coil structures. The fraction of α-helical secondary structures increased upon increasing the DP of PPLG, similar to the finding reported by Papadopoulos *et al.* for PBLG.[4] At low DPs (<18), both secondary structures were present, but as the DP increased, the α-helical secondary structure dominated. In addition, all of the PPLG-*g*-CD species obtained after the click reactions exhibited α-helical secondary structures—even those with relatively low DPs (*e.g.*, $PPLG_5$-*g*-CD). Thus, the presence of the rigid CD moieties appeared to enhance hydrogen bonding between the C═O groups and the amide linkages in the α-helical conformation.[37]

The secondary structures of PPLG also can be identified on the basis of their distinctly different signals in solid state NMR spectra.[38,39] Fig. 8 displays the ^{13}C CP/MAS spectra of PPLG and PPLG-*g*-CD at room temperature. The peak assignments are similar to those in Fig. 2, but broader bands appeared in the solid state NMR because of dipole–dipole interactions and chemical shift anisotropy. We attribute the different ^{13}C chemical shifts exhibited by the C_α and amide C═O resonances to differences in the local conformations of the individual amino acid residues, characterized in terms of dihedral angles and the types of inter- and intramolecular hydrogen bonds. In the case of PPLG, the α-helical secondary structure thaws characterized by the signals of the C_α and amide C═O resonances appearing at 57.5 and 176 ppm, respectively. In its β-sheet conformation, these signals were shifted upfield, by approximately 4–5 ppm, to 52.7 and 172 ppm, respectively.[2] Because the signals of the C_α nuclei partially overlapped with those from the CD moieties, it was easier for us to distinguish the peptide secondary structures from their distinctly different C═O resonances. Clearly, the fractions of α-helical secondary structures of the PPLG-*g*-CD systems were higher than those of the corresponding PPLG species at the same DP of the polypeptide.

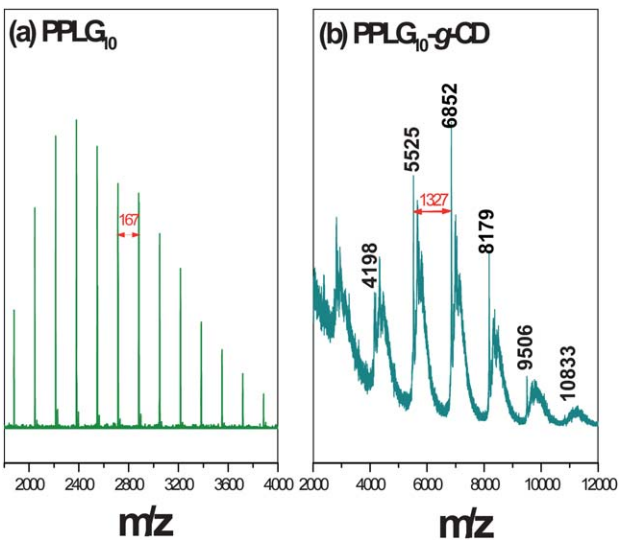

Fig. 4 MALDI-TOF mass spectra of (a) $PPLG_{10}$ and (b) $PPLG_{10}$-*g*-CD.

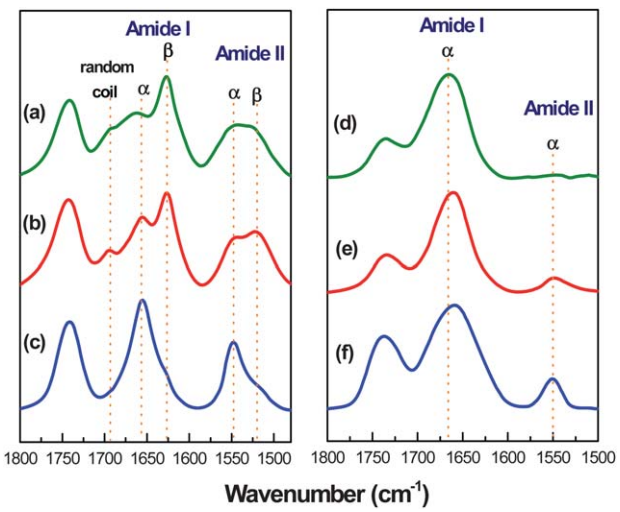

Fig. 5 FTIR spectra of (a) $PPLG_5$, (b) $PPLG_{10}$, (c) $PPLG_{30}$, (d) $PPLG_5$-*g*-CD, (e) $PPLG_{10}$-*g*-CD, and (f) $PPLG_{30}$-*g*-CD.

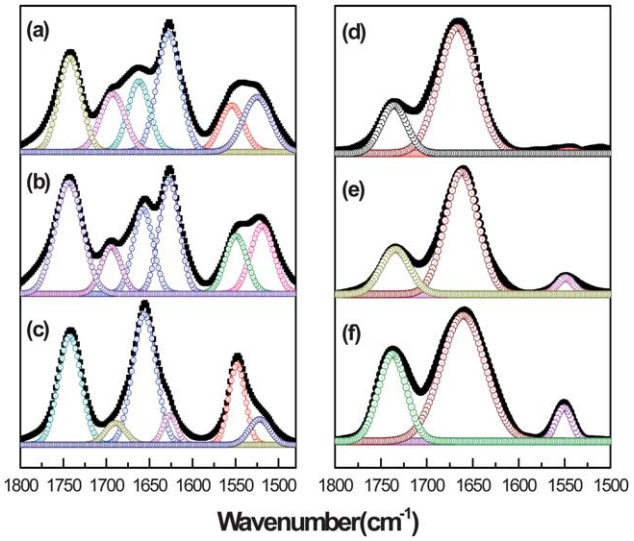

Fig. 6 Curve fitting data from the FTIR spectra of (a) $PPLG_5$, (b) $PPLG_{10}$, (c) $PPLG_{30}$, (d) $PPLG_5$-*g*-CD, (e) $PPLG_{10}$-*g*-CD, and (f) $PPLG_{30}$-*g*-CD.

We could also characterize the secondary structures of PPLG and PPLG-*g*-CD from their wide-angle X-ray diffraction patterns recorded at 393 K. For PPLG [Fig. 9(A)], the diffraction patterns at DPs of 5 and 10 revealed the presence of β-sheet secondary structures. The first peak at a value of q of 0.48 reflects the distance (d = 1.30 nm) between the backbones in the antiparallel β-pleated sheet structure; the reflection at a value of q of 1.34 (d = 4.68 nm) represents the intermolecular distance between adjacent peptide chains within one lamella. Increasing the DP of PPLG to 30 resulted in disappearance of the diffraction peak at a value of q of 0.48, associated with the β-sheet secondary structure, suggesting the absence of that particular conformation in the longer peptides. The three reflections at higher angles, with positions $1 : 3^{1/2} : 4^{1/2}$ relative to the primary peak (q*), are indexed according to the (10), (11), and (20) reflections of a 2D hexagonal packing of cylinders composed of 18/5 α-helices with a cylinder distance of 1.18 nm.[4] The structure

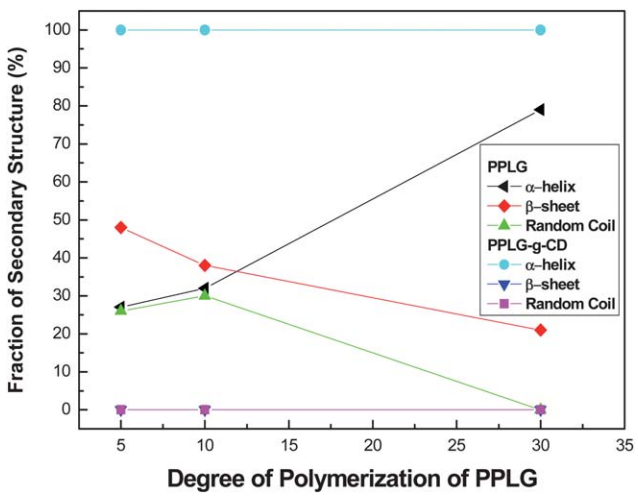

Fig. 7 Secondary structures of PPLG and PPLG-*g*-CD systems featuring different DPs.

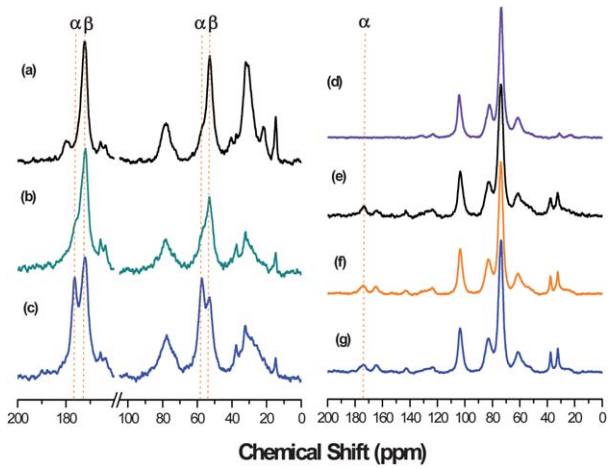

Fig. 8 Solid state ^{13}C NMR spectra of (a) $PPLG_5$, (b) $PPLG_{10}$, (c) $PPLG_{30}$, (d) β-CD-N_3, (e) $PPLG_5$-*g*-CD, (f) $PPLG_{10}$-*g*-CD, and (g) $PPLG_{30}$-*g*-CD.

of PPLG has been described as a nematic-like paracrystal with a periodic packing of α-helices in the direction lateral to the chain axis. The broad amorphous region at a value of q of 1.54 originated mainly from the long amorphous side chain. Additionally, the α-helical conformations were better packed in the longer peptide. Decreasing the length of the PPLG chain (to a DP of 5 or 10) led to destabilization of the α-helical secondary structures. The β-sheet secondary structure was represented by signals at values of q of 0.48 and 1.34.

Fig. 9(B) displays the WAXD patterns of the PPLG-*g*-CD species recorded at 393 K; these diffraction patterns exhibit dramatic differences relative to those of the PPLG systems. For a considerable fraction of the peptide segments, the sharp peak at a value of q of 1.34, corresponding to the β-sheet secondary structure, was absent when the DP of the peptide segment of PPLG-*g*-CD was less than 10. This result is different from that obtained for PPLG. Clearly, after the click reactions, the fractions of α-helical secondary structures of the PPLG-*g*-CD species were higher than those of the PPLG systems, consistent with the

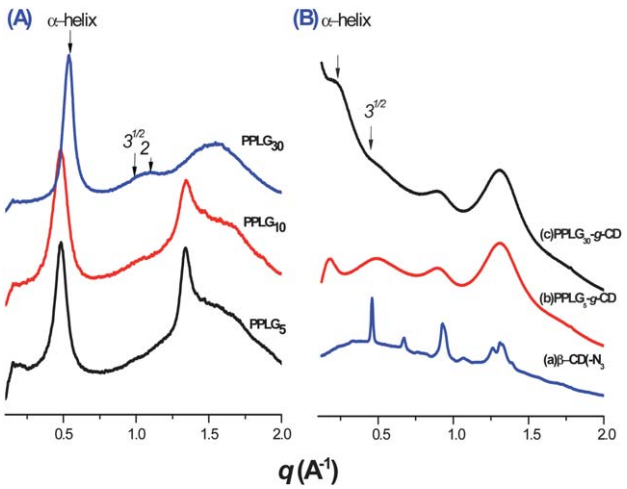

Fig. 9 WAXD patterns (recorded at 393 K) of (A) PPLG with different DPs and (B) (a) β-CD-N_3, (b) $PPLG_5$-*g*-CD, and (c) $PPLG_{30}$-*g*-CD species featuring different DPs.

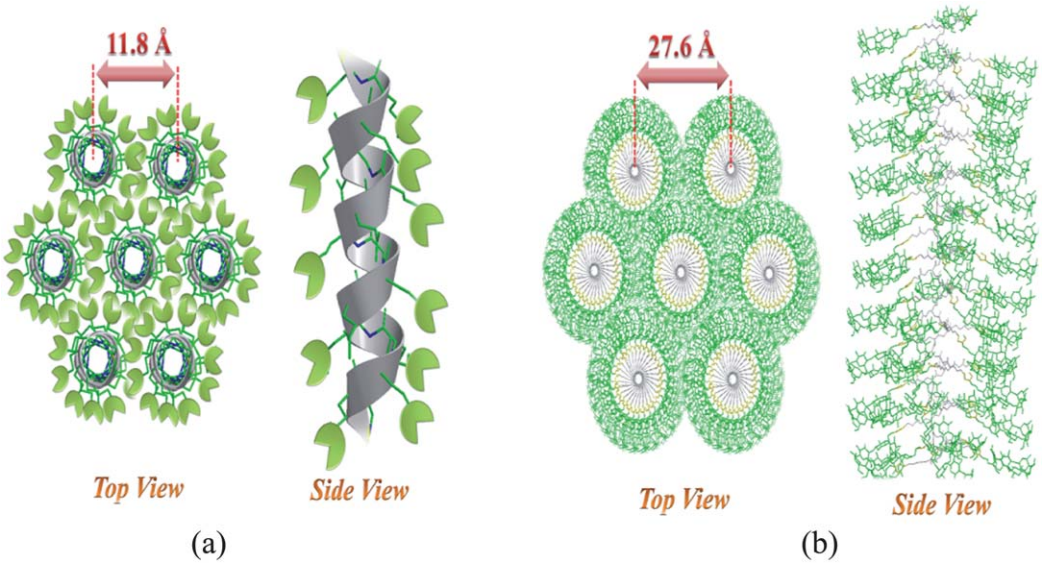

Scheme 2 Self-assembly of (a) PPLG and (b) PPLG-*g*-CD.

results of our FTIR spectroscopic analyses. As a result, we conclude that incorporation of the CD moieties on the PPLG side chains encouraged the formation of PPLG α-helices.

This conformation is stabilized through intramolecular hydrogen bonding. We infer that even if the peptides adopted both α-helical and β-sheet conformations, conformational stabilization occurred after anchoring the CD units to the side chains, resulting in most of the peptide segments becoming constrained in the α-helical secondary structure. Fig. 9(B) reveals that the WAXD pattern of $PPLG_{30}$-*g*-CD features more than one strong additional diffraction angle (at $q = 0.23$) and a weak diffraction angle (at $q = 0.40$), relative to the pattern of pure PPLG. These two reflections, with a relative position of $1 : 3^{1/2}$, correspond to 2D hexagonal packing of the cylinders of PPLG-*g*-CD. Structurally speaking, the PPLG system tethered the CD units on the side chain from its crystalline domains; meanwhile, the scattered CD moieties gathered and locked into the copolymers to form crystalline entities. Scheme 2 provides a schematic depiction of the α-helical conformation and cylindrical organization of the PPLG and PPLG-*g*-CD species. 2D hexagonal packing of cylinders appeared for PPLG with a cylinder distance of 1.18 nm [Scheme 2(a)], as calculated from the WAXD data, with a characteristic spacing (27.6 Å) representing the hexagonally packed cylinder structure of the PPLG-*g*-CD copolymer [Scheme 2(b)]. The observed spacing was equal to the thickness (27.6 Å) expected for the repeated packing of a PPLG-*g*-CD bilayer structure, as estimated from the sum of twice the CD length (2×7.9 Å $= 15.8$ Å)[32] and the cylinder distance of (11.8 Å) of PPLG (15.8 + 11.8 = 27.6 Å), as indicated in Scheme 2(b).

We recorded temperature-dependent FTIR spectra of $PPLG_{10}$ and $PPLG_{10}$-*g*-CD to obtain information regarding the conformations of their peptide segments (Fig. 10). The amide I and amide II bands at 1655 and 1545 cm^{-1}, respectively, represent the α-helical secondary structure. These bands shifted to 1626 and 1520 cm^{-1}, respectively, for the β-sheet conformation. Here, we chose to study the $PPLG_{10}$ oligomers because they possessed both α-helical and β-sheet conformations. Because the longer $PPLG_{30}$ system adopted almost entirely the α-helical secondary structure, it was insensitive to changes in temperature. The spectra of $PPLG_{10}$-*g*-CD indicated that its α-helical secondary structure was stabilized significantly after attachment of the rigid CD structures to the PPLG homopeptide. The fraction of α-helical secondary structures of $PPLG_{10}$ decreased significantly upon increasing the temperature [Fig. 10(a)], whereas the secondary structure of PPLG-*g*-CD remained almost unchanged with respect to the temperature [Fig. 10(b)]. Thus, the DP, the temperature, and the presence of CD units all strongly influenced the secondary structure. Increasing the DP for all of these polypeptides resulted in stabilization of the α-helical secondary structure. The attachment of CD moieties also stabilized the α-helical secondary structure toward increases in temperature.

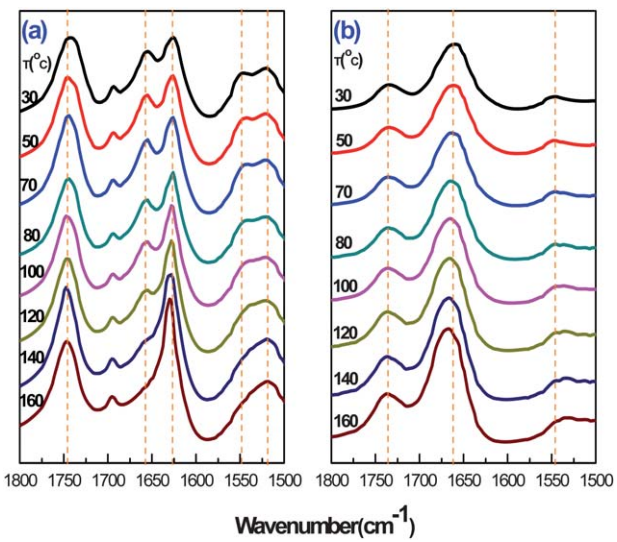

Fig. 10 Variable-temperature FTIR spectra of (a) $PPLG_{10}$ and (b) $PPLG_{10}$-*g*-CD.

We recorded circular dichroism spectra to quantify the behavior of the secondary structures of the PPLG and PPLG-*g*-CD species, dissolved in MeOH and water, respectively. The α-helical structure was characterized by a triply inflected spectrum, corresponding to two negative bands at 208 and 222 nm with almost equivalent intensities and a strong positive band at 192 nm. The β-sheet structure was characterized by a negative minimum band near 218 nm and a positive maximum near 198 nm. The random coil structure was characterized by a small positive band at 218 nm and a large negative band near 200 nm.[40] The fourth principal structure, the C_{10}-helix (*i.e.*, a repetitive hydrogen-bonded ring containing 10 atoms),[41] possesses a tighter, more-elongated, and higher potential energy than the α-helix structure (C_{13}-helix). Nevertheless, the C_{10}-helix was characterized by a small positive band at 195 nm, with a smaller intensity and a much lower ellipticity ratio ($[\theta]_{222}/[\theta]_{208}$) than that of the α-helix.[42] Fig. 11 presents the circular dichroism spectra of the PPLG and PPLG-*g*-CD species. The former revealed a transformation from the random coil to β-sheet and α-helix structures upon increasing the DP; the latter, in which CD units were grafted onto the oligomers through click chemistry, exhibited well-defined α-helices. At higher molecular weights, the PPLG-*g*-CD species exhibited greater amounts of C_{10}-helical conformations, presumably due to steric effects and noncovalent interactions among the CD units. Next, we tested the effect of pH on the conformations of our PPLG-*g*-CD systems. Fig. 12 displays the pH-induced conformational changes and self-assembly of $PPLG_{30}$-*g*-CD solutions. In acidic media, the amide groups of the polymer chains were protonated; the slight decrease in the ratio $[\theta]_{222}/[\theta]_{208}$ of $PPLG_{30}$-*g*-CD revealed that the C_{10}-helix composition was directly proportional to the acidity. Nevertheless, the polymer bioconjugate remained as a helical mixture of α-helix and C_{10}-helix structures.[40] When we dissolved $PPLG_{30}$-*g*-CD in NaOH solutions, the triply inflected spectrum reduced to a doubly inflected dichroic spectrum somewhere between pH 11 and 11.5. The α-helix of poly(L-glutamic acid) species transformed to a random coil conformation induced by ionization, with the transformation beginning at pH

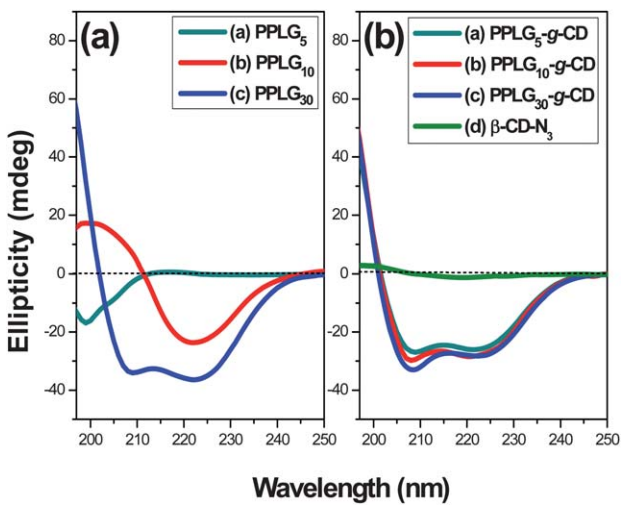

Fig. 11 Circular dichroism spectra of (a) PPLG species in neutral MeOH (1.0 mg mL^{-1}) and (b) PPLG-*g*-CD species in neutral H_2O (1.0 mg mL^{-1}).

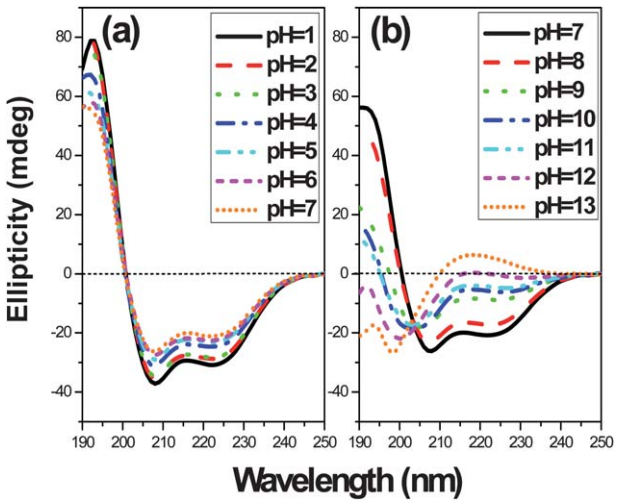

Fig. 12 Effect of pH on the circular dichroism spectrum of $PPLG_{30}$-*g*-CD in (a) HCl solution (2.0 mg mL^{-1}) and (b) NaOH solution (2.0 mg mL^{-1}).

6.18.[40,43] This phenomenon is known as the helix–coil transition. The CD moieties attached to the side chain of PPLG might prevent the electrostatic interactions of the side chains from forming extended coil conformations, because of steric hindrance or a stabilized helical conformation, at transition values of pH relatively higher than those of poly(L-glutamic acid).[40]

ICs with guest compounds

We dissolved the polypeptide–CD hybrid $PPLG_{10}$-*g*-CD and Py, a lipophilic fluorophore, at equivalent concentrations in water and THF, respectively. The host–guest interactions between the hydrophobic cavity of the β-CD units and the pyrene molecules would generate ICs after heating and ultrasonic vibration. Fig. 13 displays the fluorescence spectra in the bulk state of Py and of the $PPLG_{10}$-*g*-CD–Py ICs after excitation at 343 nm. The former exhibited signals for both the monomer (374 nm) and the fluorescent excimer (493 nm); the latter exhibited strong monomer fluorescence, but a quenched excimer fluorescence. The intensity ratio I_{476}/I_{373} decreased from 2.24 for Py to 0.07 for the ICs, presumably because the walls of the CD cavities disrupted the π–π stacking of the Py units; therefore, our proposed model consists of 1 : 1 and 2 : 1 β-CD–Py complexes.[27] Scheme 3 displays possible mechanisms and structures determined from fluorescence spectroscopic analyses.

Our other means of identification of the complexation phenomena was to measure the intensity ratio of the vibronic band I to band III, located at 374 and 385 nm individually; any variation in this value would be caused by changes in the polarity of the microenvironment. The polymer bioconjugates possessing self-assembled helical structures presenting a high density of β-CD units provided extremely hydrophilic environments for much tighter binding than that provided by monomeric complexes. The intensity ratio of the vibronic bands I and III decreased unambiguously from 0.85 for free Py to 0.68 for the ICs, because the hydrophilic OH groups of the β-CD units enhanced the intensity of the vibronic band III. These changes in fluorescence spectra confirm the success of the complexation events.[44,45]

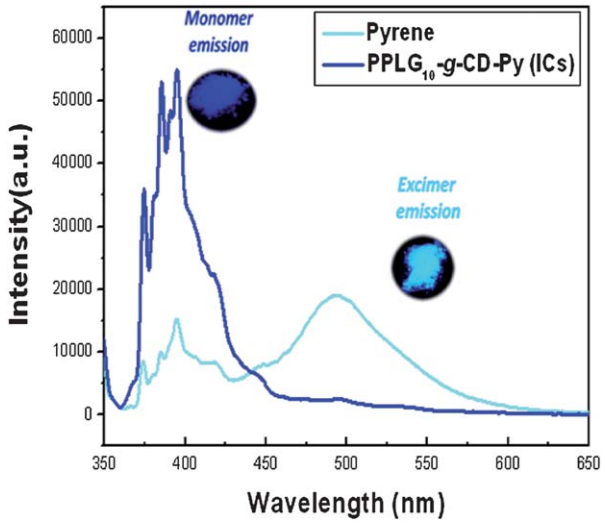

Fig. 13 Fluorescence spectra of Py and $PPLG_{10}$-*g*-CD–Py ICs in the solid state.

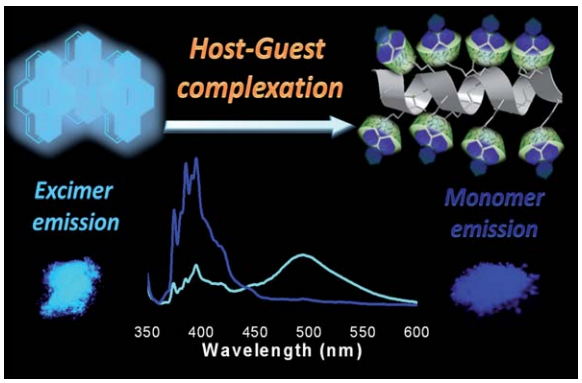

Scheme 3 Fluorescence spectra of Py and host–guest complexation between the PPLG-*g*-CD copolymer and Py.

Conclusions

We have used a combination of ring opening polymerization and click chemistry to prepare a new series of water-soluble PPLG-*g*-CD polymer bioconjugates featuring stable α-helical conformations. We have found that the DP, the temperature, and the attachment of CD units all had a strong influence on the secondary structure. Increasing the DP for all of the polypeptides resulted in stabilization of the α-helical secondary structure. Attachment of CD moieties to pure PPLG enhanced its water-solubility and also stabilized its α-helical secondary structure toward increases in the temperature or pH of the solution. In addition, the presence of CD cavities also allowed the formation of ICs with Py, suggesting potential applications for PPLG-*g*-CD species in biocompatible, biodegradable and nontoxic drug delivery carrier systems.

Acknowledgements

This study was supported financially by the National Science Council, Taiwan, Republic of China, under contracts NSC 100-2221-E-110-029-MY3 and NSC 100-2628-E-110-001.

Notes and references

1 H. A. Klok and S. Lecommandoux, *Adv. Mater.*, 2001, **13**, 1217–1229.
2 M. Sela and E. Katchalski, *Adv. Protein Chem.*, 1959, **14**, 391–478.
3 J. Kopacek, *J. Controlled Release*, 1990, **11**, 279–290.
4 P. Papadopoulos, G. Floudas, H. A. Klok, I. Schnell and T. Pakula, *Biomacromolecules*, 2004, **5**, 81–91.
5 H. A. Klok and S. Lecommandoux, *Adv. Polym. Sci.*, 2006, **202**, 75–111.
6 J. T. Yang and P. Doty, *J. Am. Chem. Soc.*, 1957, **79**, 761–775.
7 M. F. Perutz, *Nature*, 1951, **167**, 1053–1054.
8 J. H. Wang, C. C. Cheng, Y. C. Yen, C. C. Miao and F. C. Chang, *Soft Matter*, 2012, **8**, 3747–3750.
9 D. A. Prystupa and A. M. Donald, *Macromolecules*, 1993, **26**, 1947–1955.
10 A. C. Engler, D. K. Bonner, H. G. Buss, E. Y. Cheung and P. T. Hammond, *Soft Matter*, 2011, **7**, 5627–5637.
11 S. W. Kuo, H. F. Lee and F. C. Chang, *J. Polym. Sci., Part A: Polym. Chem.*, 2008, **46**, 3108–3119.
12 S. W. Kuo, H. F. Lee, W. J. Huang, K. U. Jeong and F. C. Chang, *Macromolecules*, 2009, **42**, 1619–1626.
13 C. M. Dobson, A. Sali and M. Karplus, *Angew. Chem., Int. Ed.*, 1998, **37**, 868–893.
14 C. M. Dobson, *Nature*, 2003, **426**, 884–890.
15 Y. Zhang, H. Lu, Y. Lin and J. Cheng, *Macromolecules*, 2011, **44**, 6641–6644.
16 M. Yu, A. P. Nowak and T. J. Deming, *J. Am. Chem. Soc.*, 1999, **121**, 12210–12211.
17 C. Chen, Z. Wang and Z. Li, *Biomacromolecules*, 2011, **12**, 2859–2863.
18 A. C. Engler, H. Lee and P. T. Hammond, *Angew. Chem., Int. Ed.*, 2009, **48**, 9334–9338.
19 Y. Chen, C. He, C. Xiao, J. Ding, X. Zhuang and X. Chen, *Polym. Chem.*, 2011, **2**, 2627–2634.
20 P. C. Painter, W. L. Tang, J. F. Graf, B. Thomson and M. M. Colema, *Macromolecules*, 1991, **24**, 3929–3936.
21 J. Zhang, K. Ellworth and P. X. Ma, *Macromol. Rapid Commun.*, 2012, **33**, 664–671.
22 J. X. Zhang and P. X. Ma, *Nano Today*, 2010, **5**, 337–350.
23 G. Wenz, *Angew. Chem., Int. Ed. Engl.*, 1994, **33**, 803–822.
24 C. C. Rusa, T. A. Bullions, J. Fox, F. E. Porbeni, X. Wang and A. E. Tonelli, *Langmuir*, 2002, **18**, 10016–10023.
25 D. R. Yei, S. W. Kuo, H. K. Fu and F. C. Chang, *Polymer*, 2005, **46**, 741–750.
26 M. A. Hossain, S. Matsumura, T. Kanai, K. Hamasaki, H. Mihara and A. Ueno, *J. Chem. Soc., Perkin Trans. 2*, 2000, 1527–1533.
27 K. A. Udachin and J. A. Ripmeester, *J. Am. Chem. Soc.*, 1998, **120**, 1080–1081.
28 A. Harada, J. Li and M. Kamachi, *Nature*, 1994, **370**, 126–128.
29 S. C. Chan, S. W. Kuo and F. C. Chang, *Macromolecules*, 2005, **38**, 3099–3107.
30 C. W. Tu, S. W. Kuo and F. C. Chang, *Polymer*, 2009, **50**, 2958–2966.
31 K. L. Liu, Z. Zhang and J. Li, *Soft Matter*, 2011, **7**, 11290–11297.
32 Y. C. Lin and S. W. Kuo, *Polym. Chem.*, 2012, **3**, 162–171.
33 Y. C. Lin and S. W. Kuo, *Polym. Chem.*, 2012, **3**, 882–891.
34 Y. Matsui, T. Yokoi and K. Mochida, *Chem. Lett.*, 1976, 1037–1040.
35 S. W. Kuo and C. J. Chen, *Macromolecules*, 2011, **44**, 7315–7326.
36 S. W. Kuo and C. J. Chen, *Macromolecules*, 2012, **45**, 2442–2452.
37 S. Jeon, J. Choo, D. Sohn and S. N. Lee, *Polymer*, 2001, **42**, 9915–9920.
38 S. W. Kuo and H. T. Tsai, *Polymer*, 2010, **51**, 5695–5704.
39 Y. C. Lin and S. W. Kuo, *J. Polym. Sci., Part A: Polym. Chem.*, 2011, **49**, 2127–2137.
40 J. Hwang and T. J. Deming, *Biomacromolecules*, 2001, **2**, 17–21.
41 K. Ananda, P. G. Vasudev, A. Sengupta, K. M. Poopathi, R. N. Shamala and P. Balaram, *J. Am. Chem. Soc.*, 2005, **127**, 16668–16674.
42 C. Toniolo, A. Polese, F. Formaggio, M. Crisma and J. Kamphuis, *J. Am. Chem. Soc.*, 1996, **118**, 2744–2745.
43 R. Zimmermann, T. Kratzmu, D. Erickson, D. Li, H. G. Braun and C. Werner, *Langmuir*, 2004, **20**, 2369–2374.
44 A. M. Peiia, T. Ndou, J. B. Zung and I. M. Wamer, *J. Phys. Chem.*, 1991, **95**, 3330–3334.
45 W. Xu, J. N. Demas, B. A. DeGraff and M. Whaleyt, *J. Phys. Chem.*, 1993, **97**, 6546–6554.